Glass Transition and Cold Crystallization in Carbon Dioxide Treated Poly(ethylene terephthalate)

Yeong-Tarng Shieh,[1] Yu-Sheng Lin[2]

[1]*Department of Chemical and Materials Engineering, National University of Kaohsiung, Kaohsiung 811, Taiwan, Republic of China*
[2]*Department of Chemical and Materials Engineering, National Yunlin University of Science and Technology, Douliou, Yunlin 640, Taiwan, Republic of China*

Received 29 November 2007; accepted 3 September 2008
DOI 10.1002/app.30376
Published online 8 May 2009 in Wiley InterScience (www.interscience.wiley.com).

ABSTRACT: An amorphous poly(ethylene terephthalate) (aPET) and a semicrystalline poly(ethylene terephthalate) obtained through the annealing of aPET at 110°C for 40 min (aPET-110-40) were treated in carbon dioxide (CO_2) at 1500 psi and 35°C for 1 h followed by treatment in a vacuum for various times to make samples containing various amount of CO_2 residues in these two CO_2-treated samples. Glass transition and cold crystallization as a function of the amount of CO_2 residues in these two CO_2-treated samples were investigated by temperature-modulated differential scanning calorimetry (TMDSC) and dynamic mechanical analysis (DMA). The CO_2 residues were found to not only depress the glass-transition temperature (T_g) but also facilitate cold crystallization in both samples. The depressed T_g in both CO_2-treated poly(ethylene terephthalate) samples was roughly inversely proportional to amount of CO_2 residues and was independent of the crystallinity of the poly(-ethylene terephthalate) sample. The nonreversing curves of TMDSC data clearly indicated that both samples exhibited a big overshoot peak around the glass transition. This overshoot peak occurred at lower temperatures and was smaller in magnitude for samples containing more CO_2 residues. The TMDSC nonreversing curves also indicated that aPET exhibited a clear cold-crystallization exotherm at 120.0°C, but aPET-110-40 exhibited two cold-crystallization exotherms at 109.2 and 127.4°C. The two cold crystallizations in the CO_2-treated aPET-110-40 became one after vacuum treatment. The DMA data exhibited multiple tan δ peaks in both CO_2-treated poly-(ethylene terephthalate) samples. These multiple tan δ peaks, attributed to multiple amorphous phases, tended to shift to higher temperatures for longer vacuum times. © 2009 Wiley Periodicals, Inc. J Appl Polym Sci 113: 3345–3353, 2009

Key words: crystallization; differential scanning calorimetry (DSC); glass transition; polyesters

INTRODUCTION

Poly(ethylene terephthalate) (PET) is a commercially important polymer material and is widely used in fibers, films, bottles, and plastics.[1–4] As used in the packaging industry, such as their use for carbonated drinks, it is highly desirable for PET bottles to have high barrier properties to prevent carbon dioxide (CO_2) in the carbonated drinks from being released. PET can be obtained as an amorphous solid by quenching from the melt and as a semicrystalline material by annealing. The barrier properties of PET are dependent on the crystallinity. The crystallization of PET is influenced by various factors, such as molecular weight, orientation, annealing, and crystallization conditions.[5] For example, the orientation can cause stress-induced crystallization and influence the crystallinity.[5–9] PET is a semirigid crystalline polymer with slow crystallization behavior; this usually leads to the presence of a large amount of metastable crystals or imperfect crystals that are not at thermodynamic equilibrium. A subsequent annealing or heating treatment would evolve a stable morphology from the metastable crystals accompanied by a heat release attributed to exothermic crystallization or a heat absorption attributed to endothermic relaxation or melting.

PET can be swelled and foamed, the morphology of PET can change, and the crystallization of PET can be induced in compressed CO_2 or by dissolved CO_2.[10–21] CO_2 can plasticize PET and induce crystallization at temperatures below its glass-transition temperature (T_g).[21–24] The crystallizations that could be induced by dissolved CO_2 were explained by the swelling and plasticization by CO_2, which eased the movement of the polymer chains for crystallization. To our knowledge, how dissolved CO_2 affects the glass transition and cold crystallization of PET of different crystallinities has not been reported as a

Correspondence to: Y.-T. Shieh (yts@nuk.edu.tw).
Contract grant sponsor: National Science Council of Taiwan; contract grant number: NSC 95-2221-E-224-047-MY3.

function of the amount of dissolved CO_2. In this study, a sheet of amorphous poly(ethylene terephthalate) (aPET) and a sheet of semicrystalline poly(ethylene terephthalate) obtained through the annealing of aPET at 110°C for 40 min (aPET-110-40) were treated in CO_2 at 1500 psi and 35°C for 1 h followed by vacuum treatment for various times to obtain various amounts of CO_2 residues in the two CO_2-treated PET samples. The glass transition and cold crystallization in these two CO_2-treated PET samples were investigated as a function of the amount of CO_2 residues by temperature-modulated differential scanning calorimetry (TMDSC) and dynamic mechanical analysis (DMA).

TMDSC is a recently developed technique[25–31] that superimposes a sinusoidal temperature oscillation onto a linear heating ramp of standard differential scanning calorimetry (DSC). The total heat flow can be obtained as in conventional DSC. The total heat flow can be separated into a heat-capacity-related (reversing) component and a time-dependent, nonreversing component.[25–31] The overshoot around the glass transition and cold crystallization in the CO_2-treated PET samples during TMDSC heating was clearly seen in the nonreversing curves and was investigated as a function of the amount of CO_2 residues in this study.

EXPERIMENTAL

Materials and sample preparation

aPET sheets 0.5 mm in thickness were obtained from Nan Ya Plastics Corp. (Taipei, Taiwan). The intrinsic viscosity was 0.704 dL/g. We obtained the aPET-110-40 sheets by annealing the aPET in an oven at 110°C for 40 min. The densities of aPET and aPET-110-40 were determined to be 1.333 and 1.360 g/cm^3, respectively. The volume fractional crystallinity (X_d) of aPET-110-40 was determined to be 22.1% with eq. (1):[5]

$$X_d = (d - d_a)/(d_c - d_a) \quad (1)$$

where d is the measured density of the sample, d_a is the density of amorphous PET and was taken as 1.333 g/cm^3,[28] and d_c is the density of fully crystalline PET and was taken as 1.455 g/cm^3.[5,32,33]

CO_2 treatments

The CO_2 treatments of the samples were performed in a high-pressure thermostat chamber supplied by Jeoou Rong Industrial Co., Ltd. (Kaohsiung, Taiwan) equipped with a syringe pump with a model 260D supplied by ISCO (Lincoln, NE). Samples 2 cm long and 0.5 cm wide cut from the sheets were put in a high-pressure cell located inside the thermostat chamber pressurized by the equipped syringe-type pump at 1500 psi. The chamber was controlled at 35°C throughout the treatment time of 60 min. Preliminary tests showed that, in the 60-min treatment time, the samples were able to reach the equilibrium solubility of CO_2. After the treatment, the cell was depressurized to ambient pressure for 50 s, and the samples were taken out for weight measurements. The treated samples were then put into a vacuum oven at room temperature to release the dissolved CO_2 and were weighed as a function of vacuum time. The vacuum times were 0, 6, 12, 24, 36, 48, and 72 h. The treated samples after complete evacuation of the dissolved CO_2 showed a negligible weight change as compared to original samples, which indicated that the samples were not eroded.

TMDSC analyses

We conducted the TMDSC analyses on a TA Instruments DSC-Q100 (New Castle, DE) by applying the heat-only mode by heating the sample at 2°C/min superposed with a temperature oscillation modulation with an amplitude of 0.32°C at a frequency of 1/min to obtain curves of total, reversing, and nonreversing heat flows. The quasi-isothermal mode was applied to obtain reversing heat-capacity data by isothermal heating at every 3°C increment for 10 min from 0 to 300°C. At each isothermal temperature, the heating was superposed with a temperature oscillation modulation of 0.5°C in amplitude in every 60-s cycle.

DMA

The dynamic mechanical properties were determined by a TA Instruments dynamic mechanical analyzer (DMA-2980) through the tensile mode. The heating rate was 3°C/min from 30 to 200°C and the forced vibrating frequency was 1 Hz with an oscillation amplitude of 15 μm.

RESULTS AND DISCUSSION

In this study, an amorphous PET (aPET) and an annealed PET (aPET-110-40) were treated in CO_2 at 1500 psi and 35°C for 1 h. Figure 1 shows the TMDSC reversing heat capacity in the temperature region 0–300°C for aPET and aPET-110-40. When we compared the two samples, we observed that the annealing caused PET to decrease the heat-capacity increase and the heat capacity at T_g. As shown in Figure 1, at T_g, the heat-capacity increases were 0.082 and 0.062 cal/g °C and the heat capacities were 0.38 and 0.37 cal/g °C for aPET and aPET-110-40, respectively. A decreased heat-capacity increase with aPET-110-40 was associated with an increase in the overall rigid fraction (f_r) due to the presence of

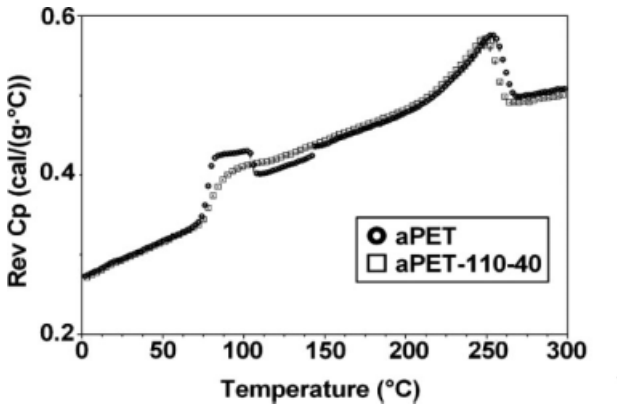

Figure 1 Reversing heat capacity (Rev C_p) of aPET and aPET-110-40 as a function of temperature.

crystallites in the sample that remained solid beyond the glass-transition region;[34] this was calculated with eq. (2):

$$f_r = 1 - (\Delta C_p / \Delta C_p^o) \quad (2)$$

where ΔC_p is the measured heat-capacity increase at T_g for a PET sample and ΔC_p^o is measured heat-capacity increase for a completely amorphous PET (0.164 cal/g °C, as determined by the difference between the glass and liquid heat capacities). By applying the ΔC_p obtained from Figure 1, we calculated the f_r values, which were 50 and 62.2% for aPET and aPET-110-40, respectively. If the two-phase crystallinity model is valid, f_r is equal to the degree of crystallinity (i.e., the crystalline fraction). If not, one finds that f_r is higher than the crystalline fraction and a rigid amorphous fraction exists between T_g and the melting temperature. The case of f_r being lower than the crystalline fraction has not been observed.[35] In this study, the degrees of crystallinity of aPET and aPET-110-40 were 0 and 22.1%, respectively, as calculated by eq. (1). Accordingly, f_r in aPET was equal to the rigid amorphous fraction in aPET. The higher f_r in aPET-110-40 compared to that in aPET reflected the presence of crystallites in aPET-110-40 in addition to the rigid amorphous fraction.

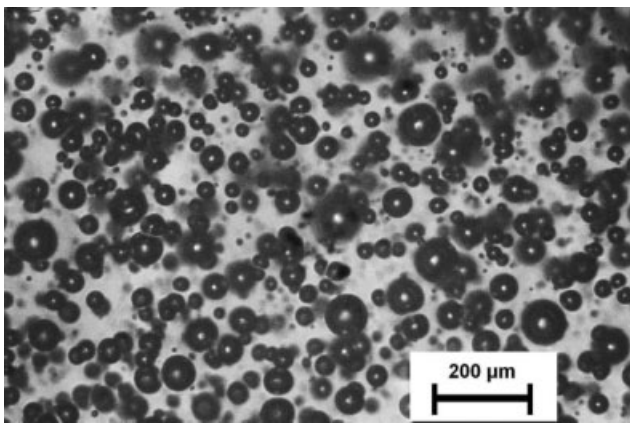

Figure 2 Optical microscopy image of CO_2-treated aPET.

TABLE I
CO_2 Residue, T_g, and T_{cc} Values of aPET and CO_2-Treated aPET as a Function of the Vacuum Time

Sample code	Vacuum time (h)	CO_2 residues (wt %)	T_g (°C)	T_{cc} (°C)
aPET,CO2,V0	0	4.31	33.2	110.5
aPET,CO2,V6	6	1.86	47.5	111.3
aPET,CO2,V12	12	1.44	53.6	112.0
aPET,CO2,V24	24	0.97	60.7	113.8
aPET,CO2,V36	36	0.74	64.1	114.2
aPET,CO2,V48	48	0.47	64.4	115.0
aPET,CO2,V72	72	0.12	67.4	115.2
aPET	—	0	74.2	120.0

The CO_2 treatment conditions were 1500 psi, 35°C, and 1 h. T_{cc} = cold-crystallization temperature.

Figure 2 shows the optical microscopy image of the CO_2-treated aPET sheet. Bubbles less than 100 µm in diameter were seen in the CO_2-treated aPET. This indicated that CO_2 could dissolve in aPET upon CO_2 treatment at 1500 psi and 35°C for 1 h. We determined the amount of dissolved CO_2 by weighing the sample immediately after the treatment. As the CO_2-treated samples were vacuumed, the amount of CO_2 residues in the samples decreased. The CO_2 weight residues in the CO_2-treated aPET sample as a function of vacuum time are tabulated in Table I, whereas those in the CO_2-treated aPET-110-40 sample are tabulated in Table II. As shown in Tables I and II, longer vacuum times caused fewer CO_2 residues in both samples, as expected. As shown in Figure 3, the amount of CO_2 residues in both samples was inversely proportional to the logarithmic vacuum time. For a vacuum time, the amount of CO_2 residues in the amorphous aPET was

TABLE II
CO_2 Residue, T_g, and T_{cc} Values of aPET-110-40 and CO_2-Treated aPET-110-40 as a Function of the Vacuum Time

Sample code	Vacuum time (h)	CO_2 residues (wt %)	T_g (°C)	T_{cc} (°C)
aPET-110-40,CO2,V0	0	3.09	43.8	73.7, 86.4
aPET-110-40,CO2,V6	6	0.94	56.3	90.1
aPET-110-40,CO2,V12	12	0.68	66.1	96.0
aPET-110-40,CO2,V24	24	0.38	67.1	98.9
aPET-110-40,CO2,V36	36	0.11	69.3	100.9
aPET-110-40,CO2,V48	48	0.04	72.4	103.2
aPET-110-40,CO2,V72	72	0	72.7	105.7
aPET-110-40	—	0	76.7	109.2, 127.4

The CO_2 treatment conditions were 1500 psi, 35°C, and 1 h. T_{cc} = cold-crystallization temperature.

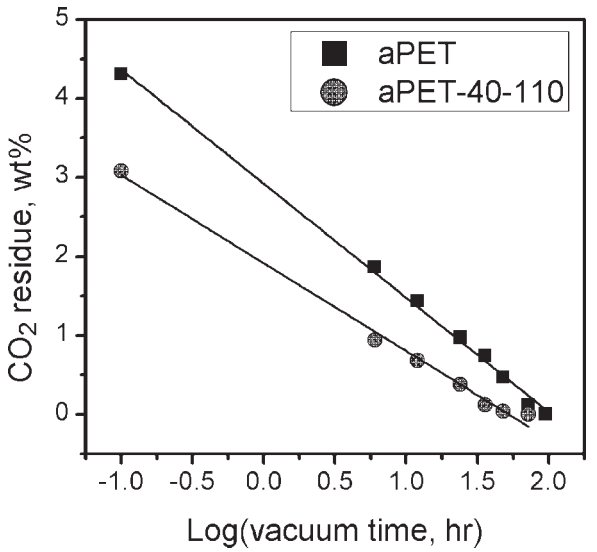

Figure 3 Amount of CO_2 residues in CO_2-treated aPET and CO_2-treated aPET-110-40 as a function of the logarithmic vacuum time.

higher than that in the crystalline aPET-110-40 with a crystallinity of 22.1%.

The TMDSC curves of the total, reversing, and nonreversing heat flows are shown in Figures 4–6, respectively, for aPET and the CO_2-treated aPET vacuumed for various times, whereas those for aPET-110-40 and the CO_2-treated aPET-110-40 are shown in Figures 7–9, respectively. As shown in Figures 4 and 7, the total heat-flow curves, similar to the conventional DSC heat-flow curves, of all of the samples exhibited glass transitions and cold crystallizations at various temperatures, in addition to a melting temperature at a roughly constant temperature of near 250°C. The glass transitions and cold crystallizations were observed at higher temperatures for samples containing fewer CO_2 residues, as shown in Tables I and II and Figure 10. This indicated that the CO_2 residues not only plasticized both samples, as shown in Figure 10 by the decreasing T_g with increasing amount of CO_2 residues, but also helped to induce cold crystallization during heating, as shown by the lower temperatures of cold crystallization for samples containing more CO_2 residues. This observation of T_g depression was attributed to an increase in free volume in the PET samples by the dissolved CO_2,[36] which eased the movement of polymer chains and, thereby, facilitated the cold crystallization.[19] In Figure 10, the depressed T_g of both CO_2-treated PET samples is shown to be roughly inversely proportional to the amount of CO_2

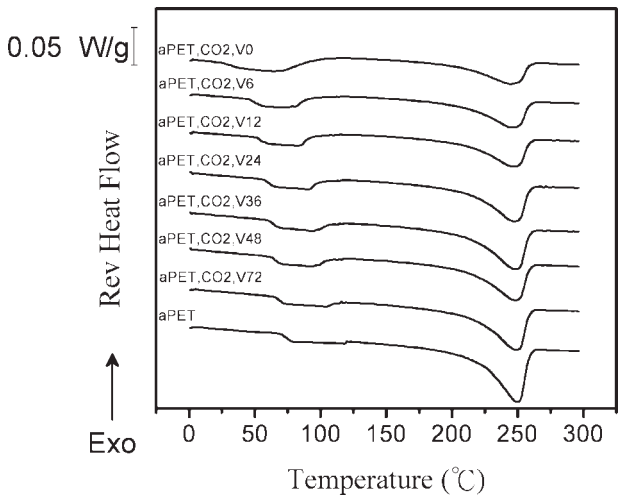

Figure 5 Reversing heat-flow curves of aPET and CO_2-treated aPET after various periods of vacuum. The amount of CO_2 residues in each sample is shown in Figure 4 and Table I.

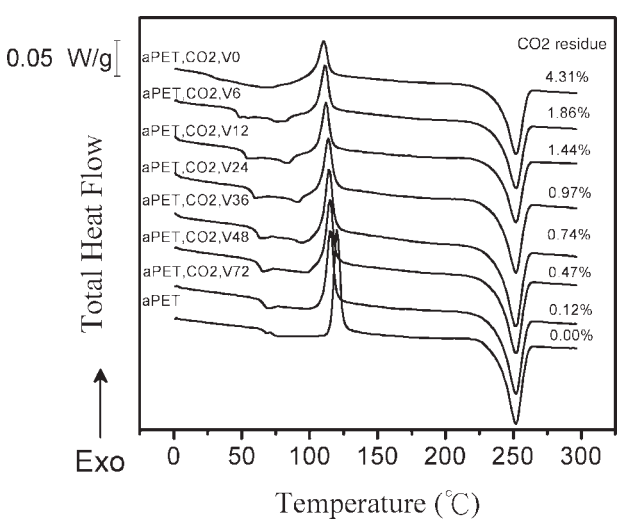

Figure 4 Total heat-flow curves of aPET and CO_2-treated aPET after various periods of vacuum.

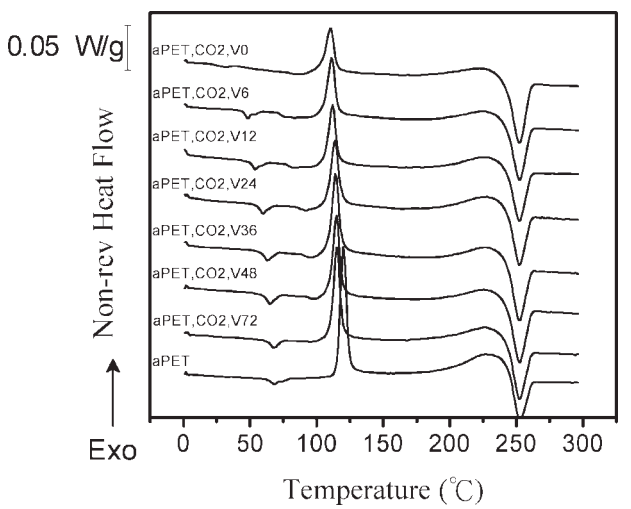

Figure 6 Nonreversing heat-flow curves of aPET and CO_2-treated aPET after various periods of vacuum. The amount of CO_2 residues in each sample is shown in Figure 4 and Table I.

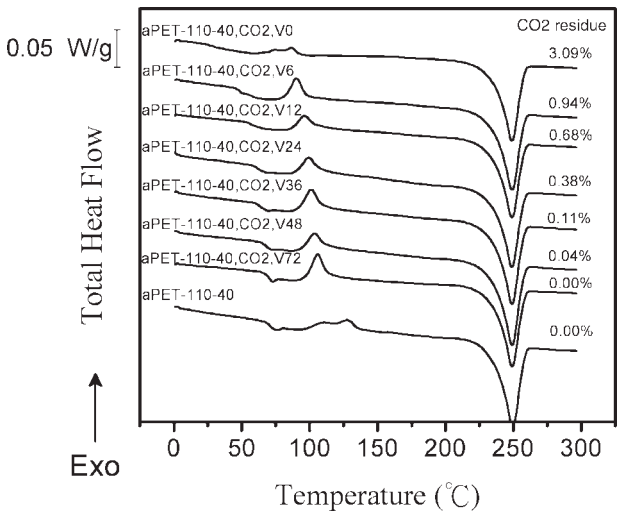

Figure 7 Total heat-flow curves of aPET-110-40 and CO_2-treated aPET-110-40 after various periods of vacuum.

residues, independent of the crystallinity of the PET sample.

As shown by the glass transition in Figure 4, which ranged from near 33°C to near 74°C for aPET and the CO_2-treated aPET samples, the total curves exhibited a heat-flow overshoot (a meltinglike endotherm) instead of a simple step inflection, which is shown in the reversing curves in Figure 5. In Figure 5, the glass transition of aPET and the CO_2-treated aPET can be recognized by a heat-capacity increase in the temperature range from near 33°C to near 74°C, followed by a heat-capacity decrease at higher temperatures due to the cold crystallization. The heat-flow overshoot during heating through the glass-transition region, as shown in the total curves in Figure 4, was due to enthalpy recovery. This was

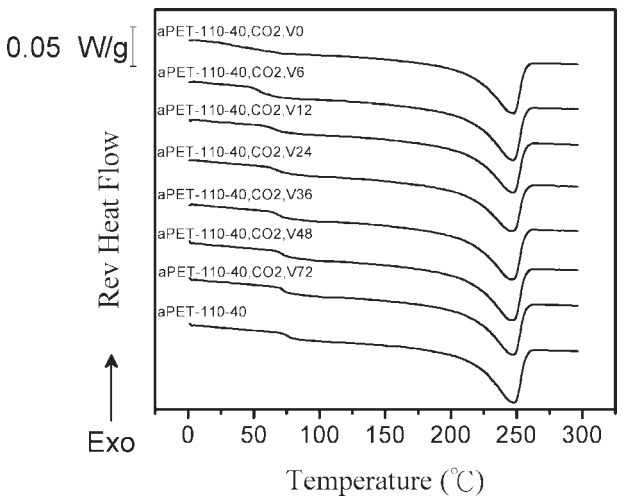

Figure 8 Reversing heat-flow curves of aPET-110-40 and CO_2-treated aPET-110-40 after various periods of vacuum. The amount of CO_2 residues in each sample is shown in Figure 7 and Table II.

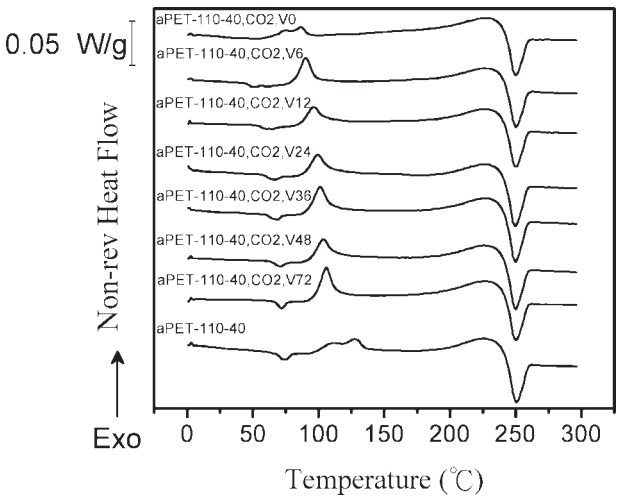

Figure 9 Nonreversing heat-flow curves of aPET-110-40 and CO_2-treated aPET-110-40 after various periods of vacuum. The amount of CO_2 residues in each sample is shown in Figure 7 and Table II.

attributed to a relaxation toward equilibrium and, thereby, a decrease in enthalpy[37–39] that occurred during the isothermal treatments in 1500-psi CO_2 at 35°C for 1 h. Because the TMDSC nonreversing heat flow (a time-dependent component) was obtained by subtraction of the reversing heat curve (a heat-capacity-related component) from the total heat flow, the nonreversing curve was more effective than the total curve for investigating the effect of the CO_2 residues on the nonequilibrium state in the sample. This effect might not be clearly monitored by conventional DSC heating but was pronounced in the nonreversing curves of the TMDSC data in this study.

In the nonreversing curves in Figures 6 and 9, the heat-flow overshoots (melting-like endotherms)

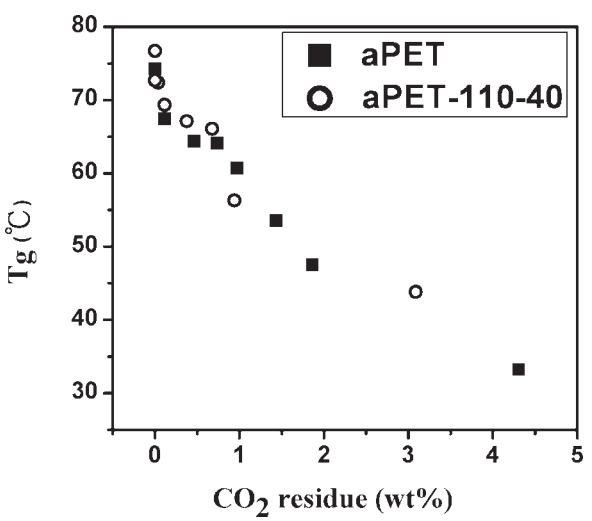

Figure 10 T_g values of CO_2-treated aPET and CO_2-treated aPET-110-40 as a function of the amount of CO_2 residues.

around the glass transitions of the samples are clearly shown, and their locations shifted to lower temperatures for samples containing more CO_2 residues. If a polymer is frozen from the melt in which the polymer chains are in a nonequilibrium state, the scanning of heat capacity upon heating around the glass transition will be a step inflection. The annealing of this polymer below T_g would relax the polymer chains toward an equilibrium state and result in a decrease in enthalpy that is recovered during heating.[37] The enthalpy recovery is visible as an endothermic peak during a DSC heating scan. Apparently, the presence of CO_2 in PET in this study helped the polymer chains relax toward an equilibrium state during the isothermal CO_2 treatments and caused a decrease in enthalpy. After the CO_2 treatments, the enthalpy of the PET samples were, thereby, seen to recover during the DSC heating, which resulted in an overshoot around T_g. The magnitudes of the overshoot peaks are shown in Figures 6 and 9 to be bigger with longer vacuum times. This was attributed to the fact that a longer vacuum time resulted in a state closer to equilibrium.

The TMDSC total curves of aPET-110-40 and the CO_2-treated aPET-110-40 shown in Figure 7 provided more information on the cold-crystallization process, which was not observed in the conventional DSC first-heating curve. The conventional DSC first-heating curve of aPET-110-40 exhibited no cold-crystallization exotherm (not shown in this article), but its TMDSC total curve exhibited two obvious exotherms near 109 and 127°C, as shown in Figure 7. In the nonreversing curves shown in Figure 9, the cold-crystallization peaks were bigger than those in the total curves. Although aPET exhibited only a cold-crystallization exotherm at 120.0°C, as shown in the nonreversing curve in Figure 6 and Table I, aPET-110-40 exhibited two distinguished cold-crystallization exotherms at 109.2 and 127.4°C, as shown in Figure 9 and Table II. This discrepancy between the two PET samples was attributed to the presence of crystallites in aPET-110-40. It is plausible that the cold crystallization in aPET-110-40 followed two processes, including a faster process occurring at a lower temperature and a slower one occurring at a higher temperature. In the presence of the crystallites, the nucleation effect enhanced the cold-crystallization rate. This resulted in a decrease in the peak temperature. The slower cold-crystallization process was related to the crystallization of free amorphous regions, and less perfect crystals might have been formed. These two cold-crystallization processes were still observed but occurred at lower temperatures of 73.7 and 86.4°C for the CO_2-treated aPET-110-40 before vacuuming. This finding suggests that the presence of CO_2 enhanced both cold-crystallization processes. These two cold-crystallization processes, however, became one after vacuuming. This was perhaps due to the fact that the release of CO_2 during vacuuming disturbed the polymer chains in the CO_2-treated aPET-110-40. The two cold-crystallization processes thus both shifted to higher temperatures, with the faster process shifting more than the slower one, and gave only one cold-crystallization exotherm.

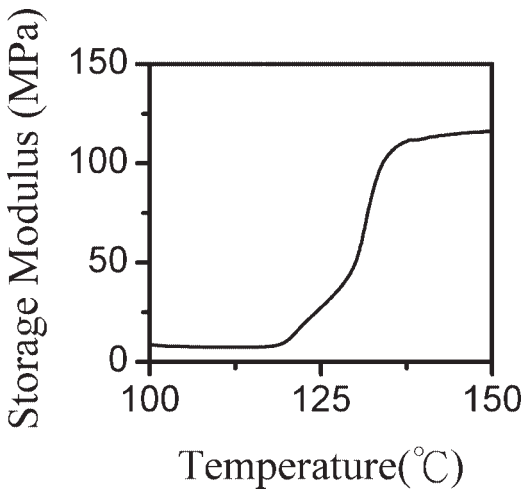

Figure 11 DMA curve of the storage modulus as a function of temperature for aPET-110-40.

The two cold-crystallization processes were also observed in the DMA data. The DMA curve of the storage modulus as a function of temperature in the 100–150°C region for aPET-110-40 is shown in Figure 11. The storage modulus increased with temperature in the region of about 120–135°C by a two-stage process. The storage modulus began to rise near 120°C with a slower increasing rate and changed to a higher increasing rate at near 130°C. This two-stage process corresponded to the double cold crystallizations observed in the TMDSC data shown in Figure 9 because the crystallinity increased upon cold crystallization and resulted in an increase in the storage modulus during DMA heating.

DMA analysis can also provide glass-transition data, and in this study, we found multiple amorphous phases in the CO_2-treated PET samples. As shown in the curves of tan δ versus temperature in Figures 12 and 13, multiple peaks were observed in the CO_2-treated aPET and CO_2-treated aPET-110-40 vacuumed for various times. These multiple tan δ peaks in the temperature region of about 48–102°C for the CO_2-treated aPET and the region of 70–100°C for the CO_2-treated aPET-110-40 were attributed to multiple amorphous phases, which formed by the dissolved CO_2 followed by vacuuming. These multiple tan δ peaks in both series of samples roughly shifted to higher temperatures for longer vacuum times. This was attributed to decreasing free

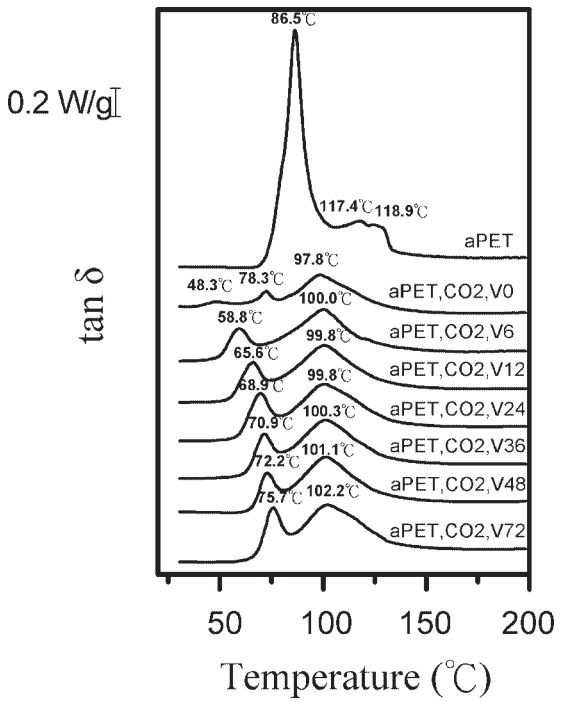

Figure 12 DMA curves of tan δ as a function of temperature for aPET and CO_2-treated aPET after various periods of vacuum. The amount of CO_2 residues in each sample is shown in Table I.

volumes in the samples with increasing vacuum times; this gave rise to decreasing CO_2 residues in samples.

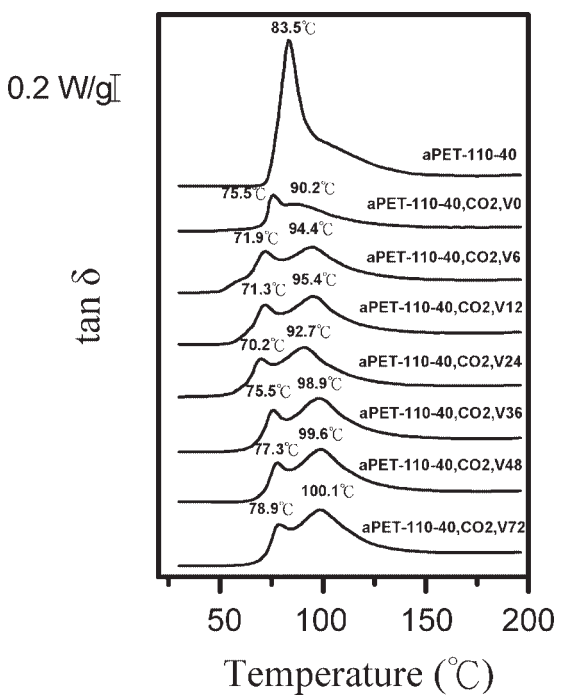

Figure 13 DMA curves of tan δ as a function of temperature for aPET-110-40 and CO_2-treated aPET-110-40 after various periods of vacuum. The amount of CO_2 residues in each sample is shown in Table II.

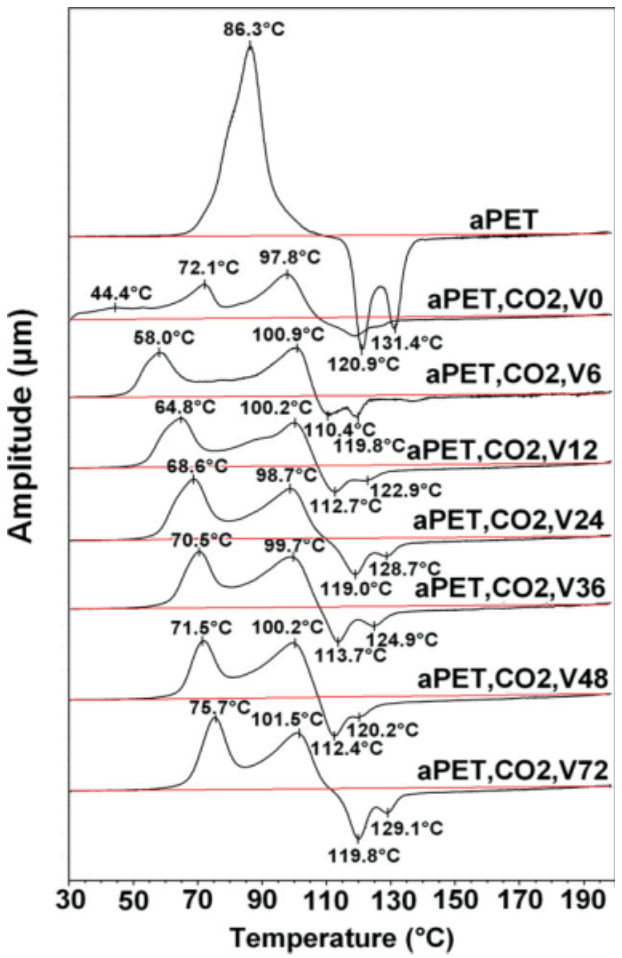

Figure 14 DMA curves of the deformation amplitude as a function of temperature for aPET and CO_2-treated aPET after various periods of vacuum. The amount of CO_2 residues in each sample is shown in Table I. [Color figure can be viewed in the online issue, which is available at www.interscience.wiley.com.]

Following the main tan δ peaks, which corresponded to the glass transitions at near 87 and 84°C for aPET and aPET-110-40, respectively, as shown in Figures 12 and 13, shoulders in the region of about 110–130°C were attributed to the cold crystallizations in aPET. The cold crystallizations, however, were not clearly observed in aPET-110-40 and any of the CO_2-treated samples in the tan δ curves shown in Figures 12 and 13. Despite the missing shoulders in Figures 12 and 13, the cold crystallizations were clearly observed for all of the samples in the curves of deformation amplitude as a function of temperature, as shown in Figures 14 and 15. To obtain the curves shown in Figures 14 and 15, a tensile stress was applied to bias the forced periodic strain, and the dynamic stress was measured to determine the dynamic mechanical properties. The static strain responded to the material properties, such as the glass transition and the crystallinity due to cold crystallization. The initial tensile deformation

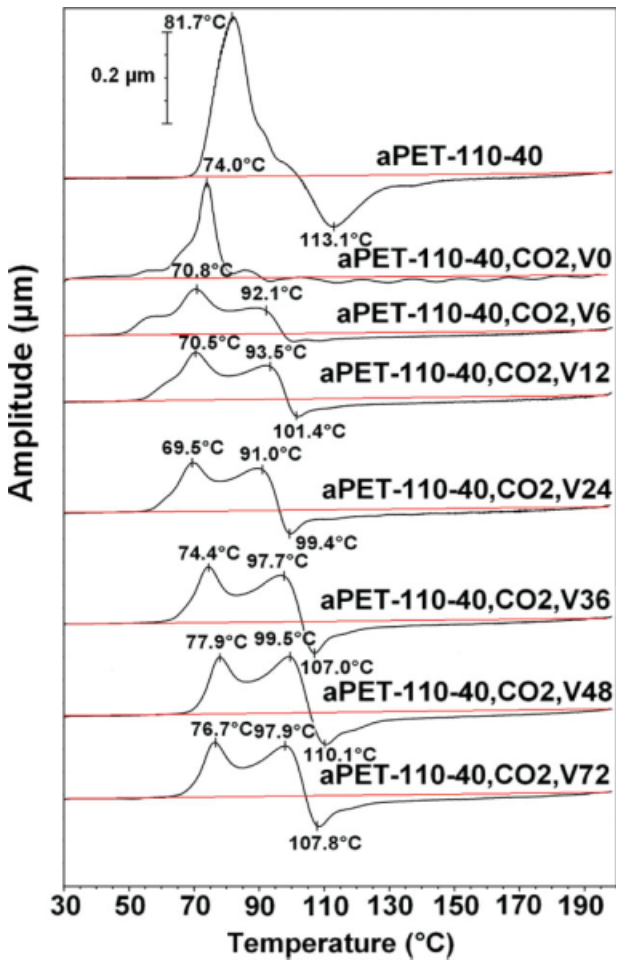

Figure 15 DMA curves of the deformation amplitude as a function of temperature for aPET-110-40 and CO_2-treated aPET-110-40 after various periods of vacuum. The amount of CO_2 residues in each sample is shown in Table II. [Color figure can be viewed in the online issue, which is available at www.interscience.wiley.com.]

amplitude was set to be 15 μm and was recorded as a function of temperature during the DMA heating. The curves of the deformation amplitude versus temperature for both the aPET and aPET-110-40 series of samples are shown in Figures 14 and 15, respectively. As shown in Figures 14 and 15, the deformation amplitudes increased around the glass transition because the materials became softer. The deformation amplitude displayed a peak for the untreated samples, and multiple peaks for the CO_2-treated samples around the glass transition responded to the lengthening of the samples. On the contrary, the modulus of the material increased as the crystallinity increased due to cold crystallization. The response was the contraction of the sample. As shown in Figures 14 and 15, aPET and the CO_2-treated aPET samples clearly exhibited two contracting peaks, whereas aPET-110-40 and the CO_2-treated aPET-110-40 samples exhibited mostly one contracting peak. We found that the two cold-crystallization processes, which could not be seen in the TMDSC data but were clearly seen in the DMA data of deformation amplitude for aPET and the CO_2-treated aPET samples, might have been associated with different characterization features between two methods. The calorimetry method (i.e., TMDSC) characterizes any process that involves heat flows, whereas the DMA method characterizes the bulk mechanical properties of a polymer.

CONCLUSIONS

Two PET samples (aPET and aPET-110-40) of different crystallinity were treated in CO_2 at 1500 psi and 35°C for 1 h followed by vacuum treatment for various times to make samples containing various amounts of CO_2 residues in these two CO_2-treated samples. The CO_2 residues were found to not only depress T_g but also facilitate cold crystallization in both samples. The depressed T_g in both CO_2-treated PET samples was found to be roughly inversely proportional to amount of CO_2 residues, independent of crystallinity of the PET sample. The nonreversing curves of the TMDSC data clearly indicated that both samples around the glass transition exhibited a big overshoot peak, which shifted to lower temperatures and became smaller in magnitude for samples containing more CO_2 residues. The TMDSC nonreversing curves also indicated that aPET exhibited a clear cold-crystallization exotherm, whereas aPET-110-40 exhibited two cold-crystallization exotherms. The two cold crystallizations in the CO_2-treated aPET-110-40 became one after vacuuming. The DMA data found that both CO_2-treated PET samples exhibited multiple tan δ peaks, which were attributed to multiple amorphous phases, and tended to shift to higher temperatures for longer vacuum times.

References

1. Goodman, I. In Encyclopedia of Polymer Science and Engineering, 2nd ed.; Mark, H. F.; Bikales, N. M.; Overberger, C. G.; Menges, G.; Kroschwits, J. I., Eds.; Wiley: New York, 1988; Vol. 12, p 1.
2. Davis, G. W.; Talbot, J. R. In Encyclopedia of Polymer Science and Engineering, 2nd ed.; Mark, H. F.; Bikales, N. M.; Overberger, C. G.; Menges, G.; Kroschwits, J. I., Eds.; Wiley: New York, 1988; Vol. 12, p 118.
3. Werner, E.; Janocha, S.; Hopper, M. J.; Mackenzie, K. J. I. In Encyclopedia of Polymer Science and Engineering, 2nd ed.; Mark, H. F.; Bikales, N. M.; Overberger, C. G.; Menges, G.; Kroschwits, J. I., Eds.; Wiley: New York, 1988; Vol. 12, p 193.
4. Jadhav, J. Y.; Kantor, S. W. In Encyclopedia of Polymer Science and Engineering, 2nd ed.; Mark, H. F.; Bikales, N. M.; Overberger, C. G.; Menges, G.; Kroschwits, J. I., Eds.; Wiley: New York, 1988; Vol. 12, p 217.
5. Khanna, Y. P.; Kuhn, W. P. In Polymeric Materials Encyclopedia; Salamone, J. C., Ed.; CRC: Boca Raton, FL, 1996; Vol. 8, p 6091.

6. Maruhashi, Y.; Asada, T. Polym Eng Sci 1996, 36, 483.
7. Ellis, J. W.; Picot, J. J. C. Polym Eng Sci 2000, 40, 1619.
8. Maruhashi, Y. Polym Eng Sci 2001, 41, 2194.
9. Zumailan, A.; Dargent, E.; Saiter, J. M. Polym Eng Sci 2004, 44, 223.
10. Hirogaki, K.; Tabata, I.; Hisada, K.; Hori, T. J Supercrit Fluids 2005, 36, 166.
11. Hirogaki, K.; Tabata, I.; Hisada, K.; Hori, T. J Supercrit Fluids 2006, 38, 399.
12. Hou, A.; Xie, K.; Dai, J. J Appl Polym Sci 2004, 92, 2008.
13. Fleming, O. S.; Kazarian, S. G. Appl Spectrosc 2004, 58, 390.
14. Smole, M. S.; Zipper, P. Int J Polym Mater 2000, 47, 681.
15. Kawahara, Y.; Kikutani, T. J Macromol Sci Phys 2000, 39, 561.
16. Bai, S.; Hu, J. Z.; Pugmire, R. J.; Grant, D. M.; Taylor, C. M. V.; Rubin, J. B.; Peterson, E. J. Macromolecules 1998, 31, 9238.
17. Brantley, N. H.; Kazarian, S. G.; Eckert, C. A. J Appl Polym Sci 2000, 77, 764.
18. Japon, S.; Leterrier, Y.; Manson, J. E. Polym Eng Sci 2000, 40, 1942.
19. Mizoguchi, K.; Hirose, T.; Naito, Y.; Kamiya, Y. Polymer 1987, 28, 1298.
20. Lambert, S. M.; Paulattis, M. E. J Supercrit Fluids 1991, 4, 15.
21. Takada, M.; Ohshima, M. Polym Eng Sci 2003, 43, 479.
22. Zhong, Z.; Zheng, S.; Mi, Y. Polymer 1999, 40, 3829.
23. Chiu, J. S.; Barlow, J. W.; Paul, D. R. Polym Eng Sci 1985, 30, 2633.
24. Chiu, J. S.; Barlow, J. W.; Paul, D. R. Polym Eng Sci 1985, 30, 3911.
25. Reading, M.; Elliott, D.; Hill, V. L. J Therm Anal 1993, 40, 949.
26. Gill, P. S.; Sauerbrunn, S. R.; Reading, M. J Therm Anal 1993, 40, 931.
27. DeClerck, K.; Rahier, H.; VanMele, B.; Kiekens, P. J Appl Polym Sci 2003, 89, 3840.
28. Bashir, Z.; Al-Aloush, I.; Al-Raqibah, I.; Ibrahim, M. Polym Eng Sci 2000, 40, 2442.
29. Okazaki, I.; Wunderlich, B. J Polym Sci Part B: Polym Phys 1996, 34, 2941.
30. Okazaki, I.; Wunderlich, B. Macromolecules 1997, 30, 1758.
31. Kampert, W. G.; Sauer, B. B. Polymer 2001, 42, 8703.
32. Mayhan, K. G.; James, W. J.; Bosch, W. J Appl Polym Sci 1965, 9, 3605.
33. Fischer, E. W.; Fakirov, S. J Mater Sci 1976, 11, 1041.
34. Cheng, S. Z. D.; Cao, M. Y.; Wunderlich, B. Macromolecules 1986, 19, 1868.
35. Cheng, S. Z. D.; Wu, Z. Q.; Wunderlich, B. Macromolecules 1987, 20, 2802.
36. Vieth, W. R.; Dao, L. H.; Pedersen, H. J Membr Sci 1991, 60, 41.
37. Bosma, M.; Brinke, G.; Ellis, T. S. Macromolecules 1988, 21, 1465.
38. Wang, Y.; Gomez Ribelles, J. L.; Salmeron Sanchez, M.; Mano, J. F. Macromolecules 2005, 38, 4712.
39. Surana, R.; Pyne, A.; Rani, M.; Suryanarayanan, R. Thermochim Acta 2005, 433, 173.